*Journal of The Electrochemical Society*, 2020 **167** 100502

# Composite Membranes Containing a Porous Separator and a Polybenzimidazole Thin Film for Vanadium Redox Flow Batteries

**Lorenz Gubler,[1,*,z] David Vonlanthen,[1,2,a,z] Aaron Schneider,[1] and Fabio J. Oldenburg[1,3]**

[1]*Electrochemistry Laboratory, Paul Scherrer Institut, 5232 Villigen PSI, Switzerland*
[2]*Swiss Battery, Dr. David Vonlanthen, 5000 Aarau, Switzerland*
[3]*Gaia Membranes, 5210 Windisch, Switzerland*

Redox flow batteries (RFBs) are energy storage devices designed for grid-scale application. For next generation RFBs it is desirable to develop low cost materials with low ohmic resistance and high transport selectivity. We present a composite membrane for the vanadium redox flow battery (VRFB) consisting of a composite of a porous polypropylene separator laminated with a thin film of polybenzimidazole (PBI). PBI layers are prepared by solution casting to obtain thicknesses in the range of 0.2 to 10 $\mu$m. The ohmic resistance of vanadium electrolyte imbibed PBI is ~50 mOhm·cm$^2$ per micrometer of film thickness at room temperature. In cell tests, composite membranes show higher coulombic efficiency compared to Nafion® 212. Composite membranes with a PBI layer thickness of 1 $\mu$m and below outperform Nafion® 212 in terms of energy efficiency and discharge capacity up to a current density of 250 mA cm$^{-2}$. With thicker PBI films the ohmic cell resistance is excessively high. Over 100 charge-discharge cycles a higher rate of capacity fading is observed for a composite membrane with 0.7 $\mu$m PBI compared to Nafion® 212, which is a result of a more pronounced net electrolyte flux from the negative to the positive electrolyte.
 [DOI: 10.1149/1945-7111/ab945f]

Manuscript submitted March 10, 2020; revised manuscript received April 11, 2020. Published May 28, 2020.

Supplementary material for this article is available online

Electrochemical energy storage technologies will help to address the problem of balancing renewable power generation and electricity grid load. Redox flow batteries (RFBs) are regarded as key stationary energy storage technology to integrate renewable solar and wind power due to the independent scalability of capacity (stored energy) and power, high cycling stability, safe operation, and the promising recycling perspective.[1] Among the various existing flow battery[2–7] and hybrid flow battery chemistries, such as the zinc/bromine,[4,8] iron/zinc,[9] and organic flow batteries,[10,11] the all-vanadium redox flow battery (VRFB) has progressed most rapidly.[12]

Currently, worldwide approximately 50% of all installed commercial flow battery systems are based on the vanadium chemistry. One of the most intriguing advantages of the VRFB is the existence of four soluble vanadium-ions with different oxidation state (II, III, IV, and V) in sulfuric acidic solution, which allows engineering a battery with a single redox-active metal on both the negative and positive side. This facilitates rebalancing and recycling of the redox-active components of the battery.

The levelized cost of storage of a stationary battery is strongly influenced by the investment cost of the system, the cycle and calendar life, and the round-trip efficiency of the battery.[13] Compared to the lithium-ion battery, the most important competitor technology, with a round trip-efficiency of 90% or more, the energy efficiency of the VRB is around 70%–75%.[14] Therefore, an increase in the round-trip efficiency of VRFB cells and batteries is highly desirable for next generation systems. Flow batteries typically use an ion exchange membrane as a polymer electrolyte. Using low-cost porous battery separators in flow batteries would lower the VRFB system cost. However, to achieve ion-selectivity, such separators need to be modified.

Recently, a number of approaches have been pursued to obtain novel flow battery membranes consisting of an asymmetric membrane architecture,[15,16] or a porous support coated with a thin layer of polymer to provide vanadium barrier properties.[17–19] Polybenzimidazole (PBI) has been a membrane material of growing interest for application in the VRFB.[20] PBI has a high chemical stability and suggests itself for use in the strongly oxidative and acidic electrolyte that is used in the VRFB. In contact with aqueous sulfuric acid, it takes up electrolyte, whereby the imidazole groups are protonated and the polymerbackbone becomes positively charged.[21] Recently, Henkensmeier and co-workers have demonstrated a layered composite membrane for the VRFB consisting of a porous PVDF film, onto which a thin, dense layer of PBI is sprayed.[18] PBI layer thicknesses were from 1.2 to 4.0 $\mu$m, which yielded an area resistance of the bilayer membrane at room temperature of 60 to 120 mΩ·cm$^2$ in 2 M sulfuric acid. Upon addition of vanadium-ions to the electrolyte, the conductivity drops by a factor of ~2.

In this study, we demonstrate a membrane architecture for the VRB based on thin PBI films with thickness range from 0.2 to 10 $\mu$m, supported on a porous polyolefin substrate of 30 $\mu$m thickness. With a low PBI film thickness and a concomitantly low ohmic resistance, the cell current density can be enhanced at a given round trip efficiency, hence increasing the power density of the cell. On a technical scale, this helps to reduce the size of the VRB stack for a target power rating, which effectively leads to a decrease of the investment cost.[22] Moreover, the absence of fluorine atoms in the membrane can facilitate recycling efforts of cell components at the end of life.

The cost of a standard polyolefin separator for application in a rechargeable battery is in the range of a few dollars per m$^2$. The cost of a porous asymmetric PBI membrane of ~70 $\mu$m thickness for VRFB application has been estimated by Yuan et al. to be less than \$50/m$^2$.[15] Considering the lower areal weight of PBI used in our approach, we estimate that the manufacturing cost of the composite membrane could be in the range of \$20/m$^2$.

## Experimental

***Materials and chemicals.—****Meta*-polybenzimidazole (mPBI) film of 70 $\mu$m thickness, in the following just referred to as "PBI," was kindly donated to PSI in 2011 by BASF Fuel Cell (Germany). The PBI was manufactured by the polyphosphoric acid process.[23] Carbon felt electrodes were purchased from Toyobo (Japan), type AAF304ZS, with a nominal thickness of 4.3 mm according to the data sheet and used without further treatment. Hydrophilic microporous polyethylene (PE), Evopor™ 5E02A (thickness: 30 $\mu$m, porosity: 75%) was purchased from Lydall Performance Materials (The Netherlands), and hydrophobic

*Electrochemical Society Member.
[a]Present address: Swiss Battery, 5000 Aarau, Switzerland.
[z]E-mail: lorenz.gubler@psi.ch; David.Vonlanthen@gmail.com

microporous polypropylene (PP), TreoPore® PDA-30 (thickness: 30 $\mu$m, porosity: >60%), from Treofan (Germany). The vanadium electrolyte was purchased from Oxkem (United Kingdom) and was composed of 1.6 M vanadium with an average oxidation number of +3.5 (formal state of charge of –50%) in 2.0 M sulfuric acid and 0.5 M phosphoric acid. For chemical stability tests, an Oxkem electrolyte with 1 M vanadium in 2 M $H_2SO_4$ was used. The V (+V) solution was prepared by electrolysis in the single cell. *N*,*N*-dimethylacetamide (DMAc) (99%) was bought from Sigma-Aldrich.

***Preparation of PBI films.***—A 10 wt-% solution of PBI was prepared by dissolving 25 g of air dried PBI film strips in 225 g DMAc. Dissolution was achieved by constantly stirring the mixture with a magnetic stir bar at 60 °C. After 8 h a clear beige-brown solution was obtained, which was filtered through a glass filter (Puradisc 25 GF 0.7 $\mu$m) each time before use. The solution was kept for two weeks. Conventional glass plates were used as substrate for coating. The glass plates were cleaned using an ultrasonic bath with (i) diluted soap solution, (ii) milliQ-water, and (iii) isopropanol. An air gun was used each time before coating to remove dust particles. A coating machine from Zehntner (Switzerland), model ZAA 2600, was used to prepare PBI films by doctor blading. Four-sided stainless steel applicators were purchased from Biuged (China). Individual slit heights between 5 and 150 $\mu$m were used to adjust the film thickness. A defined amount of 10 wt-% PBI solution was placed on the glass substrate, and the coating was performed with a constant speed of 25 mm $s^{-1}$ at room temperature. Subsequently, the coated plates were placed in an oven for 30 min at 150 °C to evaporate the solvent. After cooling to room temperature in air, the coated glass plates were immersed in deionized water for 10–30 min. Depending on the thickness and thus mechanical robustness of the film, an extra transfer method was needed for films with thickness below 1 $\mu$m to ensure the film stays smooth and crease-free. For this, the films were peeled off, so that they would float on the water surface. A sheet of hydrophilic porous PE (Evopor™) was used to cover the floating PBI film and as soon as the PE was wetted, the PBI film and PE, adhering to each other, were removed with tweezers for drying in air. Films thicker than 1 $\mu$m could be removed without mechanical support.

***Curing of PBI films.***—Upon immersion in acid, the as-prepared membranes disintegrated. Therefore, they were subjected to a curing step to improve stability. The free-standing PBI films were placed between two glass fiber filters for curing at 350 °C in air in a muffle furnace. Curing of PBI membranes has been reported in the context of their use in high-temperature polymer electrolyte fuel cells to improve their physico-chemical properties, such as higher mechanical toughness and improved radical-oxidative resistance.[24,25] In the work reported here, different curing times were used for films of different thickness (cf. Supplementary Information, Section S1 is available online at stacks.iop.org/JES/167/100502/mmedia). Overcuring resulted in oxidation of the polymer, indicated by darkening of the film.

***Lamination of composite membranes.***—PBI films (ca. 8 cm × 8 cm) were hotpressed with a microporous separator between two PTFE sheets at 80 °C at a pressure of 40 kN/2.3–2.4 MPa for 10 min. For all battery performance measurements, hydrophobic PP supports (TreoPore® PDA-30) were used, and hydrophilic PE supports (Evopor™ 5E02A) for the measurement of the membrane resistance (cf below). Figure 1 shows a PBI film of 2.7 $\mu$m thickness laminated with the porous PP support.

***Membrane characterization.***—The thickness of the PBI films was determined using a surface profilometer (Dektak 8 Advanced Development Profiler, Veeco, United States). The thickness was determined at least at 3–6 positions on a 5 cm × 5 cm dry film. The through-plane resistance of composite membranes was measured in a homemade Swagelok cell (cf. Supplementary Information, Section S2).

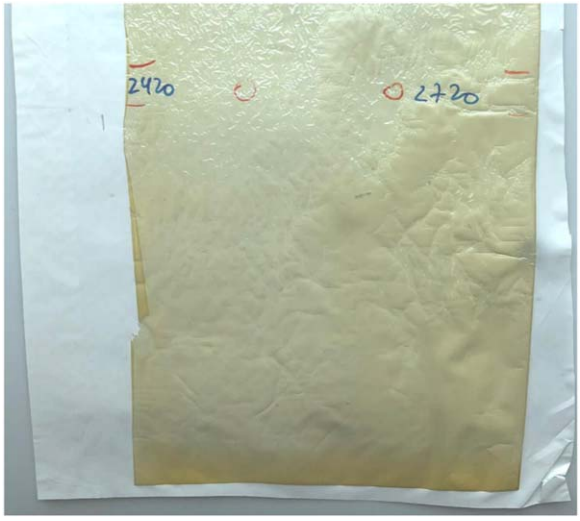


**Figure 1.** Free-standing PBI film of 2.7 $\mu$m thickness laminated at 80 °C to a porous polypropylene support (TreoPore® PDA-30, 30 $\mu$m) to obtain a composite bilayer membrane.

For acid-doping, a PE-PBI bilayer was covered with another hydrophilic PE separator, and the trilayer sandwich was punched out to give a PE-PBI-PE stack with a diameter of 8 mm. This was then placed on a clean glass plate, soaked with vanadium electrolyte, and covered with a top glass plate. The PBI film was thus acid-doped overnight (16 h). To measure the through-plane resistance, one PE-separator was carefully removed and the remaining wet PE-PBI bilayer was assembled into the measurement cell. The resistance was measured by electrochemical impedance spectroscopy in the frequency range 1 MHz–0.5 Hz, and the high frequency intercept with the real axis in the Nyquist plot was taken as the ohmic resistance. Electrolyte-filled PE separators without PBI film were analyzed to determine the baseline resistance of the substrate.

***Cell tests.***—For in situ characterization of membranes, single cells with graphite triple-serpentine flow field plates and an active area of 25 $cm^2$ were used (flow-by setup). Carbon felt electrodes from Toyobo (Japan), type AAF304ZS, were used as received. The compression was adjusted using plastic frames of different thickness. The composite membrane was assembled into the cell with the PBI layer facing the negative electrode. In previous studies using PBI-Nafion® 212 bilayer membranes,[21] we did not see an influence of the orientation on the performance. The measured ohmic resistance of the cell strongly depends on the compression (cf. Supplementary Information, Fig. S3). The standard electrode compression used was 28%. The PP-PBI composite membranes were wetted in ethanol before assembly to improve the wettability in the cell with electrolyte. The 8 bolts of the cell were tightened to 4 Nm and the cell assembled into a Scribner Model 857 test stand (Scribner Associates, USA) with glass electrolyte reservoirs designed in-house. 40 or 60 ml of vanadium electrolyte from Oxkem (United Kingdom) was used. The flow rate of electrolyte was 50 ml $min^{-1}$ on both sides. Plasticizer-free Tygon® 2100 tubes (Cole-Parmer, Germany) were used. The in situ through-plane area resistance was determined initially while flowing the vanadium electrolyte with state of charge of –50% through the cell using electrochemical impedance spectroscopy. Impedance spectra were recorded between 100 kHz and 10 mHz at zero DC current and a perturbation amplitude of 100 mV. The ohmic resistance was obtained from the high-frequency intercept of the impedance spectrum in the Nyquist diagram with the real axis. The measurement was carried out after 4 h equilibration with electrolyte. The initial charging of the battery was performed at a current density of 40 mA $cm^{-2}$. Charge/discharge cycling tests were carried out with

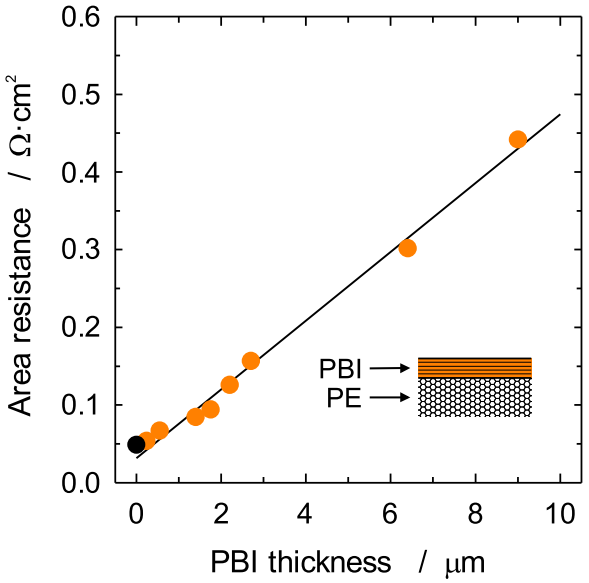


**Figure 2.** Area specific resistance (through-plane) measured at room temperature of a series of bilayers of PBI films of different dry thickness supported on a porous substrate (hydrophilic polyethylene, Evopor™ 5E02A, Lydall Performance Material, The Netherlands). The black symbol represents the measurement with the PE substrate only (49.3 ± 0.3 mΩ·cm$^2$), which has not undergone hotpressing. The samples were doped in vanadium electrolyte (1.6 M $V^{+3.5}$ in 2 M $H_2SO_4$ and 0.5 M $H_3PO_4$) for 16 h at room temperature prior to the measurement. For experimental details, cf. Supporting Information, Section S2.

0.8 V and 1.65 V as the lower and upper voltage limit, respectively. From charge/discharge curves at constant current $I$ and the measured cell voltage $U$ as a function of time $t$, the coulombic efficiency $\varepsilon_C$, voltage efficiency $\varepsilon_V$, and energy efficiency $\varepsilon_E$ were calculated according to:

$$\varepsilon_E = \frac{\int_0^{t_d} I \cdot U(t) \cdot dt}{\int_0^{t_c} I \cdot U(t) \cdot dt} = \frac{\overline{U_d}}{\overline{U_c}} \cdot \frac{t_d}{t_c} = \varepsilon_V \cdot \varepsilon_C \qquad [1]$$

where $\overline{U}$ is the average voltage and the subscripts "c" and "d" stand for "charge" and "discharge," respectively. A "static cell" setup without circulation of electrolyte was used to measure self-discharge curves and perform an extended charge/discharge test of 2'800 cycles. 3.8 ml (nominal capacity: 163 mAh) electrolyte was injected to each of the two cell compartments with a syringe. An SP-300 potentiostat with an internal 10 A booster from BioLogic (Germany) was used in combination with the static cell. For the charge/discharge experiment over 2'800 cycles, a tube connecting the two compartments was introduced to prevent build-up of internal pressure due to electrolyte transport effects across the membrane. This also leads to a continuous reflow of electrolyte to minimize capacity fading as a result of electrolyte imbalance. All measurements were performed at room temperature.

***Oxidative stability.***—To assess the oxidative stability of the PBI films in the charged electrolyte, two samples of a 3 $\mu$m PBI film where immersed in a solution of 1 M $VO_2^+$ in 2 M $H_2SO_4$ at 22 °C for 1 d and 140 d, respectively. Afterwards, the samples were washed thoroughly with 2 M $H_2SO_4$ and deionized water until a neutral pH was observed. Subsequently, the membranes were dried at 50 °C in vacuum and analyzed using ATR-FTIR spectroscopy (Bruker Vertex V70 spectrometer with a Bruker Platinum ATR Diamond set-up).

## Results and Discussion

The coating procedure of PBI films using the coating machine and solutions of controlled concentration yielded polymer films with consistent thickness after drying. Examples of measured thickness average and standard deviation for a range of PBI films are shown in the Supplementary Information, Table SII. The relative uncertainty ranges from 5% for the thinnest film (0.22 $\mu$m) to 1% for the thickest one (10 $\mu$m).

***Ex situ ohmic resistance.***—PBI films with thickness in the range of 0.24 to 9.0 $\mu$m laminated to a porous hydrophilic PE support were doped in vanadium electrolyte overnight and then assembled into the Swagelok cell to determine the area specific resistance via electrochemical impedance spectroscopy. The results in Fig. 2 indicate a steady increase of the ohmic resistance of the PE-PBI bilayer membrane as a function of the dry PBI film

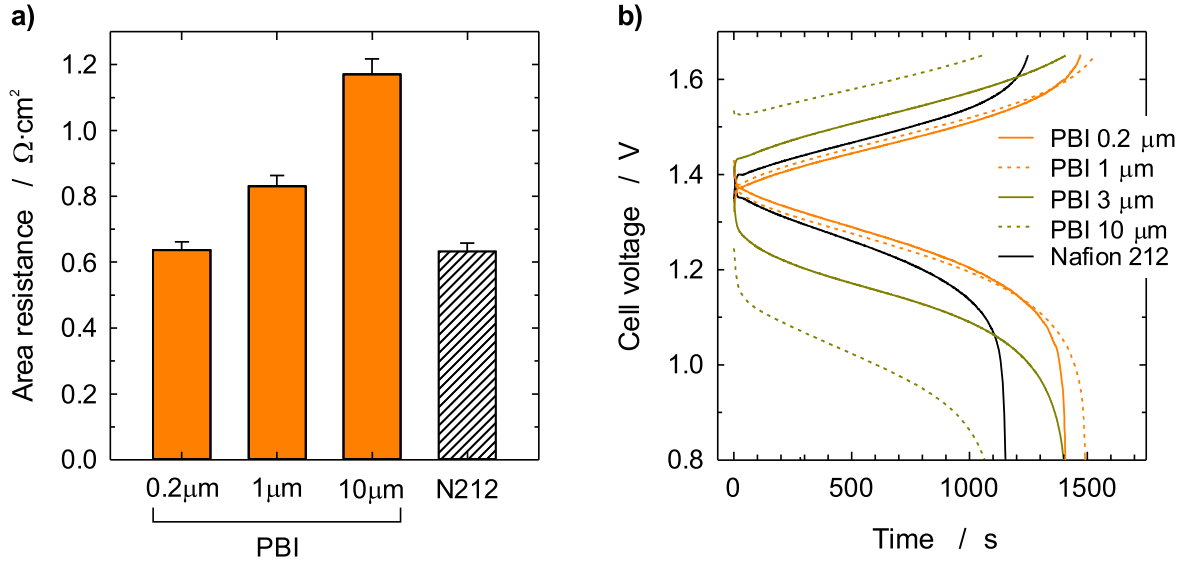


**Figure 3.** (a) Area specific resistance measured in situ after conditioning of the cell for 4 h in $V^{+3.5}$ electrolyte (state of charge of –50%). (b) Charge/discharge curves recorded at room temperature and a current density of 150 mA·cm$^{-2}$. Electrodes: Toyobo AAF304ZS (compression: 28%). 40 ml of vanadium electrolyte on each side (nominal capacity: 1.72 Ah), flow rate: 50 ml·min$^{-1}$.

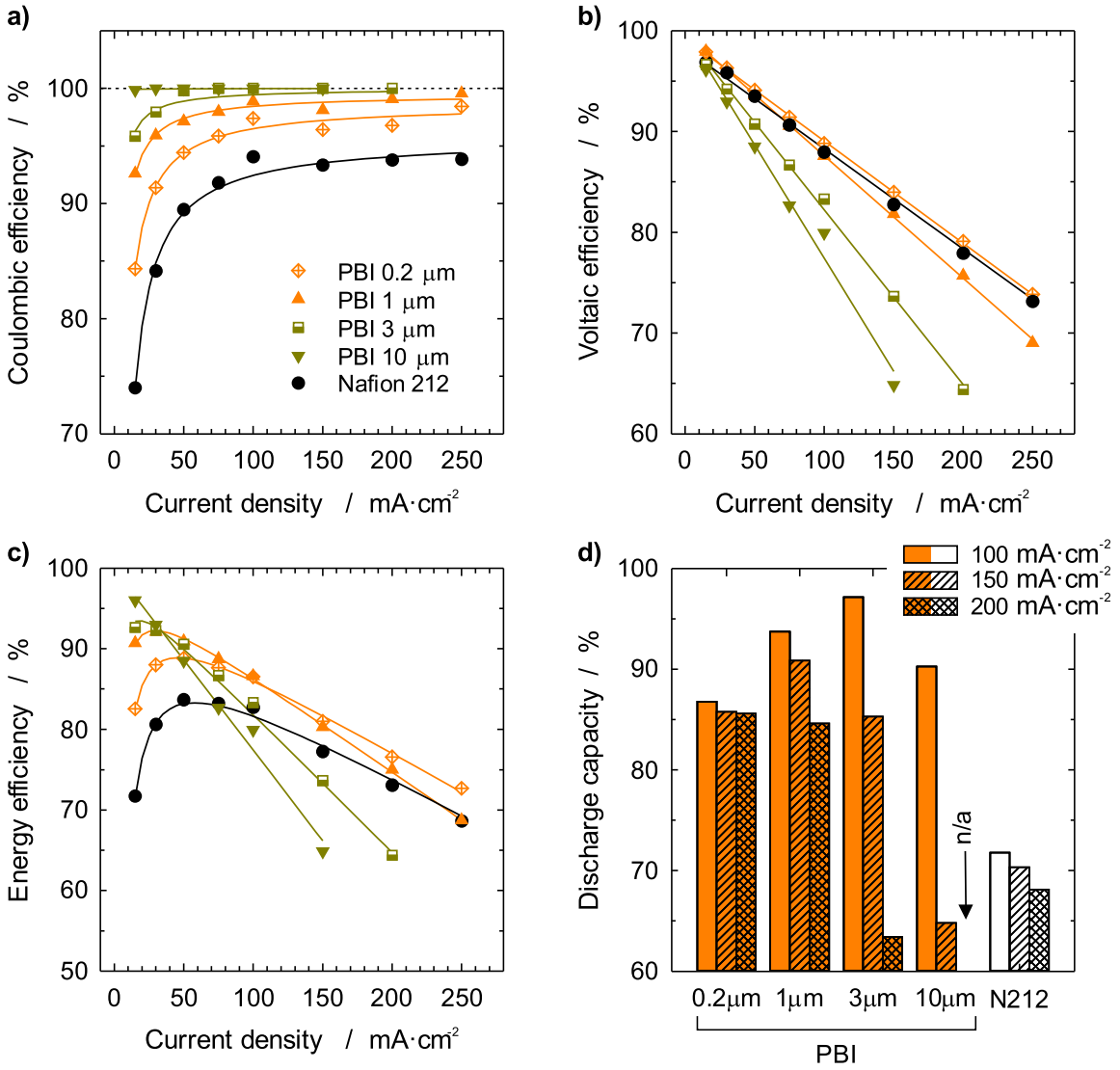


**Figure 4.** (a)–(c) Charge/discharge cycling efficiencies as a function of current density. The solid lines are fits based on a s simple model (cf. Supplementary Information, Section S5) (d) discharge capacity at selected current densities (nominal capacity: 1.72 Ah).

thickness. A linear regression analysis yields an increase in the ohmic resistance of 44 ± 2 mΩ·cm$^2$ per micrometer of dry PBI film thickness. Hence, for a target maximum ohmic resistance contributed by the PBI layer that is similar or better than that of Nafion® 212, the film thickness should not exceed ∼2 $\mu$m. Furthermore, from the slope of the regression line a conductivity of the acid doped PBI of 2.3 ± 0.1 mS cm$^{-1}$ is obtained. This value is based on the dry film thickness, and we have to take into consideration the expansion of the polymer film upon doping with acid, which is about 15% in thickness direction. With this correction, an effective conductivity value of acid doped PBI membranes of 2.0 ± 0.1 mS cm$^{-1}$ is obtained. When equilibrated in 2 M sulfuric acid, the conductivity is ∼1.6 times higher than when equilibrated in vanadium electrolyte (measured using a composite membrane with PBI layer thickness of 1.4 $\mu$m). Those conductivity values are generally in good agreement with literature. For example, Glipa et al. reported a conductivity of 2–3 mS cm$^{-1}$ for a PBI membrane doped in 2 M sulfuric acid,[26] and Noh et al. measured 4.9 mS cm$^{-1}$ for mPBI doped with 2 M sulfuric acid.[20]

***Single cell testing.***—Composite membranes using porous polypropylene (TreoPore®) and PBI films of different thickness were assembled into single cells with carbon felt electrodes from Toyobo. For initial conditioning, the starting vanadium electrolyte with an average vanadium oxidation number of +3.5, corresponding to an effective state of charge of –50%, was pumped through the positive and negative cell compartment. At the same time, the ohmic resistance of the cell was measured intermittently. A drop in resistance was observed over the first 1 to 2 h, which is attributed to the wetting of the electrochemically active materials. After the value had stabilized, the ohmic resistance measurement was taken after 4 h (Fig. 3a). We see that for a cell resistance comparable to the one obtained with Nafion® 212, a PBI thickness of below 1 $\mu$m is required. A sizeable fraction of resistance in the cell of ∼0.45 Ω·cm$^2$ is attributed to non-membrane contributions, such as the electrolyte, electrodes and contact resistances. From the increase of the ohmic resistance with PBI (dry) film thickness, a conductivity of 2.1 ± 0.5 mS cm$^{-1}$ is obtained. This is, within the margin of error, identical to the value determined ex situ in the Swagelok cell (Fig. 2). However, the resistance does not show a linear relation with

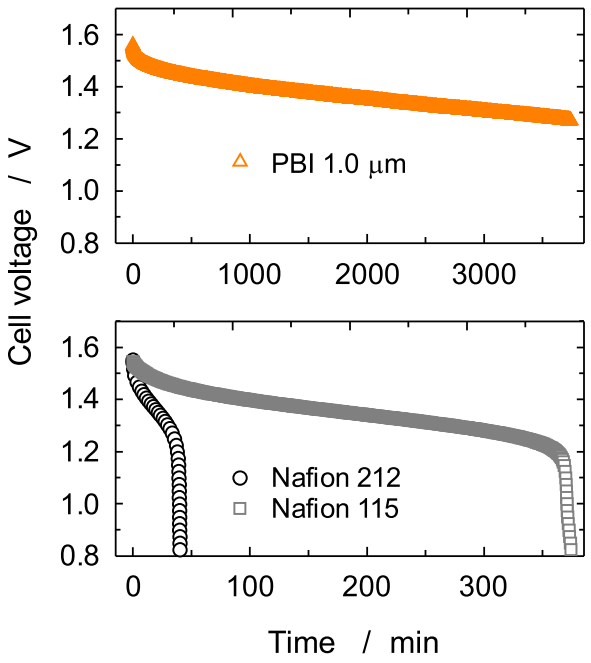


**Figure 5.** Self discharge test in the static cell with 3.8 ml electrolyte used on each side. The cell was initially charged to 1.65 V at a current density of 40 mA $cm^{-2}$ and then held at 1.65 V for another 30 min before commencing the self discharge test at open circuit voltage (OCV).

the PBI thickness. The reason is unclear at present. It may be related to different structural properties of the PBI resulting from its specific method of preparation, especially the drying and curing stage (cf. Supplementary Information, Section S1).

After the conditioning with the $V^{+3.5}$ electrolyte flowing through the cell, the battery was charged at a current density of 40 mA $cm^{-2}$ to a cell voltage of 1.65 V. Subsequently, charge/discharge profiles were measured at different current density. The charge/discharge curves for the different samples at a representative current density of 150 mA $cm^{-2}$ are shown in Fig. 3b. Curves at other current densities using 1 $\mu$m PBI and Nafion® 212 can be found in the Supplementary Information, Fig. S4. The curves show that composite membranes up to a PBI thickness of 1 $\mu$m show better performance than Nafion® 212, i.e., a lower cell voltage during charge and a higher cell voltage during discharge. Samples with PBI thickness of 3 and 10 $\mu$m show inferior performance as a result of high ohmic resistance. With the composite membranes, higher discharge capacity is obtained compared to Nafion® 212 except for the sample with 10 $\mu$m thick PBI. Here, the lower voltage limit of 0.8 V is reached after shorter time due to higher overpotentials.

From the charge/discharge cycles at current densities ranging from 50 to 250 mA $cm^{-2}$, the coulombic, voltage and energy efficiency, and the discharge capacity were calculated (Fig. 4). As expected, the coulombic efficiency increases with increasing PBI layer thickness. Even the composite with a 0.2 $\mu$m thick PBI membrane showed a coulombic efficiency that was on average 5% higher than that obtained with Nafion® 212. In addition, the voltaic efficiency shows the expected trend with PBI thickness if the overpotential is dominated by the ohmic resistance $R_\Omega$. As the difference in voltage $\Delta U$ between the charge and discharge polarization curve increases with current density according to $\Delta U = 2 \cdot i \cdot R_\Omega$, the voltaic efficiency decreases about linearly with current density $i$. The combined effect of coulombic and voltaic efficiency is shown in the energy efficiency curves. Losses at low current density are dominated by the coulombic efficiency, whereas at high current densities they are dominated by the voltaic efficiency. Overall, the composite membranes with PBI film thicknesses of 0.2 and 1.0 $\mu$m show superior performance compared to Nafion® 212 in the explored current density range up to 250 mA $cm^{-2}$. Discharge capacities are shown at selected current densities as bar graph. Overall, PP-PBI composite membranes yield a superior capacity utilization, except for the samples with PBI thickness of 3 and 10 $\mu$m. Here, the lower voltage limit of 0.8 V is reached prematurely, owing to the lower discharge voltage caused by high ohmic resistance.

***Self-discharge curves.***—In an initially fully charged "static" cell without flowing electrolyte, the continuous crossover of vanadium-ions through the membrane leads to a gradual discharge. The state of charge is correlated, according to the Nernst equation, with the measured open circuit voltage (OCV). A steep drop in OCV occurs when all of the V(II) and V(V) are consumed. The time it takes for this to happen, evidently, is a measure for the vanadium barrier properties of the membrane. Figure 5 shows that with Nafion® 212 the cell is self-discharged after 40 min, which, taking into consideration the nominal capacity of 163 mAh in the 3.8 ml of electrolyte, corresponds to a self-discharge current density $i_x$ of ~10 mA $cm^{-2}$. With Nafion® 115, the self-discharge time is ~380 min, which is actually much more than what would be expected from the difference in thickness (50 vs 150 $\mu$m). Using the composite membrane with 1 $\mu$m thick PBI, the self-discharge test was performed for 3'700 min (~62 h) and then discontinued, without having observed a complete discharge at the end of test. This illustrates the superior vanadium barrier properties of the PBI-based composite membrane. It is evident, however, that the transport of vanadium-ions and the other electrolyte constituents by diffusion alone does not reflect the situation encountered in an operating cell. The effect of migration and (electro)osmosis can be significant and dominant, especially at high current densities, as will be shown below. In addition, the permeability values of the 4 vanadium-ions can be quite different.[27] Nevertheless, results of self-discharge curves can give a general trend of how easily vanadium-ions pass through the membrane.

***Extended cycling.***—The cell performance in terms of efficiency and available discharge capacity was investigated over 100 charge-discharge cycles for a composite membrane with 0.73 $\mu$m PBI layer thickness in comparison to a Nafion® 212 membrane (Fig. 6). In analogy to the results shown in Fig. 4, the cell with composite membrane shows a higher coulombic efficiency, which is a result of the superior vanadium barrier properties. The voltage efficiency, which is indicative of the ohmic resistance of the membrane and cell, is of comparable magnitude. The resulting energy efficiency is higher by 3.6 ± 0.9% over the 100 cycles for the composite membrane. The discharge capacity shows a considerably different trend: initially, the discharge capacity was 90 to 95% of the nominal capacity. Upon cycling, the capacity fades for both cells, yet with a higher rate for the cell with the composite membrane. After 100 cycles, ~40% of the capacity is maintained with the cell with Nafion® 212 and only ~20% for the one with the composite membrane. The difference is a result of dissimilar rates of net electrolyte transfer between the positive and negative electrolyte compartment, which causes capacity imbalance. The difference in electrolyte volume between the positive and negative side was 22 ml and 54 ml in case of the cell with Nafion® 212 and the composite membrane, respectively, after 100 cycles, which explains the difference in measured discharge capacity. For both cells, the volume of the positive electrolyte increased over that of the negative electrolyte. This is expected for a cation exchange membrane. For an anion exchange membrane, a net electrolyte transfer from the positive to the negative side is expected.[27] However, it has been shown that the direction of net vanadium flux can be reversed with increasing current density.[21] Also, it has to be considered that the electrolyte uptake properties of PBI are distinctively different to those of a regular anion exchange membrane.[28] In any case, the results indicate that further development is necessary regarding the structure of the PBI layer, which is subject to future studies, to

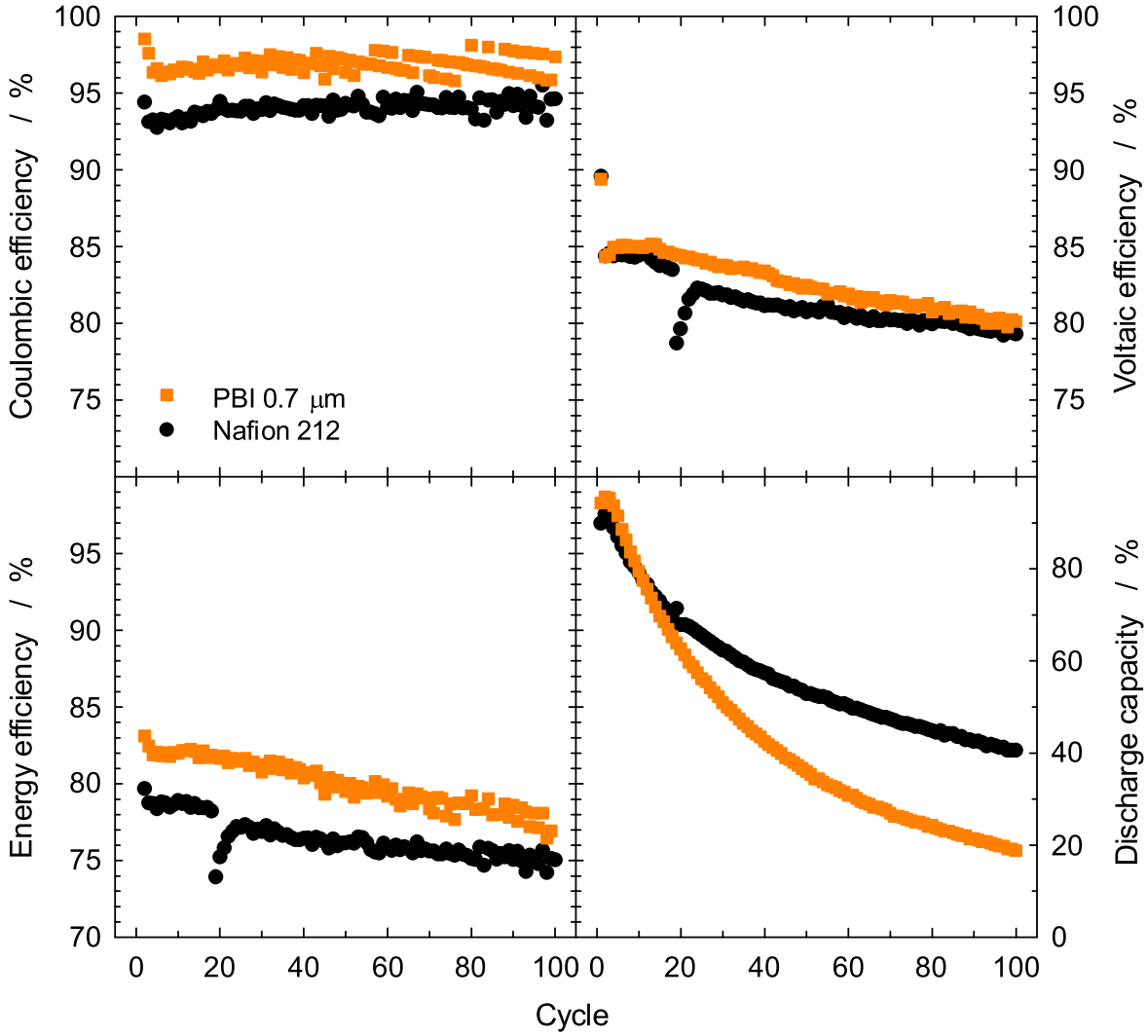


**Figure 6.** Charge/discharge cycling tests at a current density of 120 mA·cm$^{-2}$. Electrodes: Toyobo AAF304ZS (compression: 28%). 60 ml of vanadium electrolyte on each side (nominal capacity: 2.57 Ah), flow rate: 60 ml·min$^{-1}$.

reduce electrolyte transfer under the influence of the electric field while maintaining or improving the conductivity of the material. This may be tackled by modifying the PBI, for example by introducing fixed ionic charge carriers[29,30] and/or crosslinkers.[31]

Extended cycles avoiding imbalance effects in electrolyte tanks were conducted in the static cell (Fig. 7). The current density was gradually ramped up from 40 to 120 mA cm$^{-2}$. The cell showed a stable energy efficiency of 80% over 2'860 cycles. Although the test only lasted for ~170 h, it shows the capability of stable extended cycling performance.

***Oxidative stability.***—The oxidative stability of PBI films was assessed by comparing the chemical constitution of two PBI films exposed to a solution of 1 M $VO_2^+$ in 2 M $H_2SO_4$ for 1 d and for 140 d. The comparison of the ATR-FTIR absorption spectra reveals only a small change in the degree of protonation: the vibrational absorption at 2500 cm$^{-1}$ correlating to the $N^+$-H-group is slightly more intense after 140 d (Fig. 8). In accordance, also the intensity of absorption bands correlating to the bisulfate ion observed in the range of 750–1200 cm$^{-1}$ were found to be increased. Traces that would result from a polymer oxidation reaction (reduced intensity of characteristic peaks, –COOH– or –COH– vibrational bands) were not detected, indicating stability of the PBI-films over the period of the experiment. Others have studied the chemical stability of PBI in the context of the application in the VRFB by exposure to $VO_2^+$ in sulfuric acid at room temperature for several months and found PBI and Nafion® to be of similar high chemical stability.[28,32]

## Conclusions

Composite membranes with asymmetric architecture consisting of a porous polyolefin separator and a thin topcoat of PBI with thickness in the micrometer range are of potential interest as separator in next generation vanadium redox flow batteries. Membranes with a PBI layer thickness below 1.5 $\mu$m swollen in vanadium electrolyte show an ohmic resistance similar or lower than that of Nafion® 212. In the single cell, those membranes outperform Nafion® 212 in terms of charge-discharge cycling efficiency in the entire current density range investigated (up to 250 mA cm$^{-2}$), largely caused by improved vanadium barrier properties leading to high coulombic efficiency. Furthermore, initial discharge capacity is higher, yet the composite membranes show more pronounced capacity fading compared to Nafion® 212, which is a result of a higher net electrolyte flux from the negative to the positive electrolyte. This calls for further development of the material, aimed at chemically modifying the PBI. The neat PBI used in this study showed no signs of oxidative degradation when exposed to 1 M $VO_2^+$ electrolyte at room temperature for 140 d.

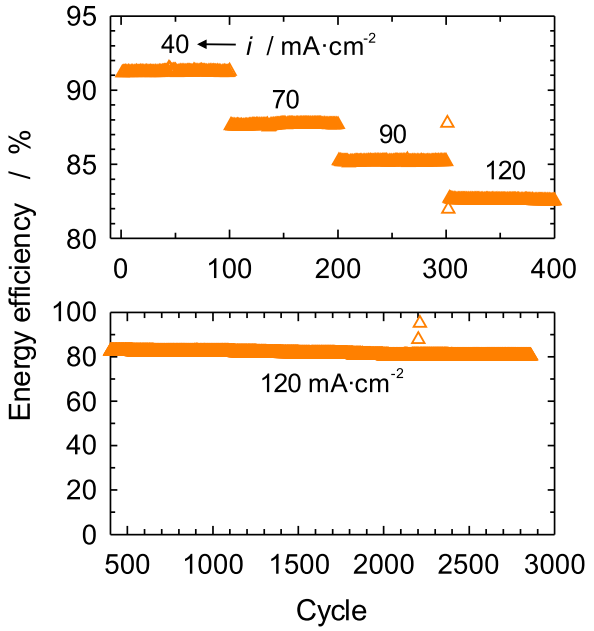


**Figure 7.** Charge/discharge cycling at different current densities using a composite membrane with a PBI layer thickness of 1.0 $\mu$m. Static cell with 3.8 ml electrolyte volume on each side.

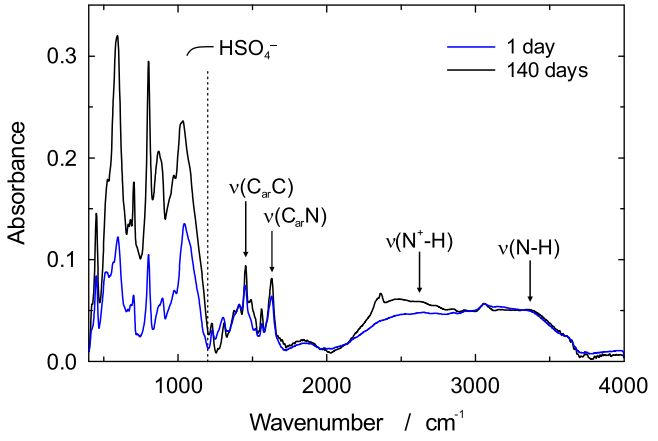


**Figure 8.** ATR-FTIR spectra of a 3 $\mu$m PBI film after being exposed to a solution of 1 M $VO_2^+$ in 2 M $H_2SO_4$ at 22 °C for 1 d (blue) and 140 d (black). Peak assignment was based on previous work.[33,34]


## Acknowledgments

This research work is supported by the Swiss National Science Foundation and Innosuisse in the framework of the Bridge Discovery program (grant number 40B2–0_176653).



## ORCID

Lorenz Gubler https://orcid.org/0000-0002-8338-6994
David Vonlanthen https://orcid.org/0000-0002-7639-3846
Fabio J. Oldenburg https://orcid.org/0000-0001-5827-9786


## References


1. B. Dunn, H. Kamath, and J.-M. Tarascon, *Science*, **334**, 928 (2011).
2. A. Z. Weber, M. M. Mench, J. P. Meyers, P. N. Ross, J. T. Gostick, and Q. Liu, *J. Appl. Electrochem.*, **41**, 1137 (2011).
3. Á. Cunha, J. Martins, N. Rodrigues, and F. P. Brito, *Int. J. Energy Res.*, **39**, 889 (2015).
4. G. L. Soloveichik, *Chem. Rev.*, **115**, 11533 (2015).
5. C. Ponce de León, A. Frías-Ferrer, J. González-García, D. A. Szánto, and F. C. Walsh, *J. Power Sources*, **160**, 716 (2006).
6. W. Wang, Q. Luo, B. Li, X. Wei, L. Li, and Z. Yang, *Adv. Funct. Mater.*, **23**, 970 (2013).
7. M. Park, J. Ryu, W. Wang, and J. Cho, *Nat. Rev. Mater.*, **2**, 16080 (2016).
8. S. Barnartt and D. A. Forejt, *J. Electrochem. Soc.*, **111**, 1201 (1964).
9. Z. Yuan, X. Liu, W. Xu, Y. Duan, H. Zhang, and X. Li, *Nat. Commun.*, **9**, 3731 (2018).
10. B. Huskinson, M. P. Marshak, C. Suh, S. Er, M. R. Gerhardt, C. J. Galvin, X. Chen, A. Aspuru-Guzik, R. G. Gordon, and M. J. Aziz, *Nature*, **505**, 195 (2014).
11. D. G. Kwabi et al., *Joule*, **2**, 1894 (2018).
12. L. Li et al., *Adv. Energy Mater.*, **1**, 394 (2011).
13. O. Schmidt, S. Melchior, A. Hawkes, and I. Staffell, *Joule*, **3**, 81 (2019).
14. Electricity Storage and Renewables: Costs and Markets to 2030, International Renewable Energy Agency (IRENA), accessed August 2018, www.irena.org.
15. Z. Yuan, Y. Duan, H. Zhang, X. Li, H. Zhang, and I. Vankelecom, *Energy Environ. Sci.*, **9**, 441 (2016).
16. S. Peng, X. Yan, X. Wu, D. Zhang, Y. Luo, L. Su, and G. He, *RSC Adv.*, **7**, 1852 (2017).
17. I. S. Chae, T. Luo, G. H. Moon, W. Ogieglo, Y. S. Kang, and M. Wessling, *Adv. Energy Mater.*, **6**, 1600517 (2016).
18. W. Lee, M. Jung, D. Serhiichuk, C. Noh, G. Gupta, C. Harms, Y. Kwon, and D. Henkensmeier, *J. Membr. Sci.*, **591**, 117333 (2019).
19. R. Tan et al., *Nat. Mater.*, **19**, 195 (2020).
20. C. Noh, M. Jung, D. Henkensmeier, S. W. Nam, and Y. Kwon, *ACS Appl. Mater. Interfaces*, **9**, 36799 (2017).
21. F. J. Oldenburg, E. Nilsson, T. J. Schmidt, and L. Gubler, *ChemSusChem*, **12**, 2620 (2019).
22. M. L. Perry and A. Z. Weber, *J. Electrochem. Soc.*, **163**, A5064 (2015).
23. L. Xiao, H. Zhang, E. Scanlon, L. S. Ramanathan, E.-W. Choe, D. Rogers, T. Apple, and B. C. Benicewicz, *Chem. Mater.*, **17**, 5328 (2005).
24. D. Aili, L. N. Cleemann, Q. Li, J. O. Jensen, E. Christensen, and N. J. Bjerrum, *J. Mater. Chem.*, **22**, 5444 (2012).
25. D. Joseph, N. N. Krishnan, D. Henkensmeier, J. H. Jang, S. H. Choi, H.-J. Kim, J. Han, and S. W. Nam, *Journal of Materials Chemistry A*, **5**, 409 (2017).
26. X. Glipa, B. Bonnet, B. Mula, D. J. Jones, and J. Rozière, *J. Mater. Chem.*, **9**, 3045 (1999).
27. F. J. Oldenburg, T. J. Schmidt, and L. Gubler, *J. Power Sources*, **368**, 68 (2017).
28. M. Jung, W. Lee, C. Noh, A. Konovalova, G. S. Yi, S. Kim, Y. Kwon, and D. Henkensmeier, *J. Membr. Sci.*, **580**, 110 (2019).
29. Y. Lee, S. Kim, A. Maljusch, O. Conradi, H.-J. Kim, J. H. Jang, J. Han, J. Kim, and D. Henkensmeier, *Polymer*, **174**, 210 (2019).
30. L. Wang, A. T. Pingitore, W. Xie, Z. Yang, M. L. Perry, and B. C. Benicewicz, *J. Electrochem. Soc.*, **166**, A1449 (2019).
31. Z. Chang, D. Henkensmeier, and R. Chen, *ChemSusChem*, **10**, 3193 (2017).
32. X. L. Zhou, T. S. Zhao, L. An, L. Wei, and C. Zhang, *Electrochim. Acta*, **153**, 492 (2015).
33. G. A. Griffin, F. Conti, S. Lavina, A. Majerus, G. Pace, C. Korte, W. Lehnert, and V. Di Noto, *Int. J. Hydrogen Energy*, **39**, 2776 (2014).
34. R. Bouchet and E. Siebert, *Solid State Ionics*, **118**, 287 (1999).

# Supplementary Information

## Composite Membranes Containing a Porous Separator and a Polybenzimidazole Thin Film for Vanadium Redox Flow Batteries

Lorenz Gubler, David Vonlanthen, Aaron Schneider, Fabio J. Oldenburg

## S1. Curing of PBI Films

The coated and dried films were cured at 350°C at various times in an aired muffle furnace (**Figure S1**) to remove the residual high-boiling-point solvent and improve the cycling stability of the ultrathin PBI membranes in the cell. Due to the varying thickness of the polymer films, different curing times where chosen (**Table S1**). The listed curing times were optimized such that the PBI polymer was not overcured, indicated by a darkening of the film.

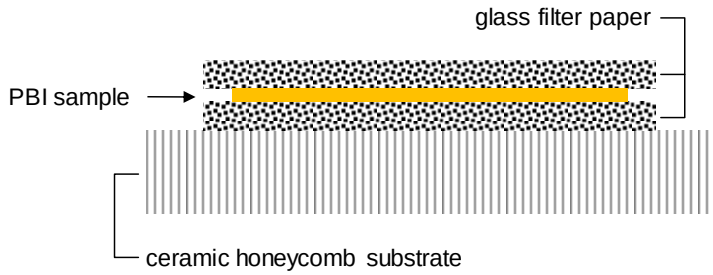


**Figure S1.** Schematic setup for curing of PBI films.

**Table S1.** Curing time (350°C, air) and dry thickness PBI films.

| PBI thickness range (□m) | Curing time (s) |
|---|---|
| < 0.3 | 30 |
| 0.3 – 0.5 | 50 |
| 0.5 – 1.5 | 60 |
| 1.5 – 2.5 | 120 |
| 2.5 – 6 | 180 |
| 6 – 9 | 240 |
| 9 – 11 | 270 |

## S2. *Ex Situ* Though-plane Resistance Measurement

A homemade Swagelok cell (**Figure S2a**) was built with PFA fittings and two stainless steel (1.4404 / 316L) cylinders (diameter 8.0 mm) to measure the trough-plane resistance of the thin-film membranes. To overcome the challenge of maintaining the acid doping of the membrane, an electrolyte-filled hydrophilic porous PE support was used to provide an electrolyte reservoir during the entire measurement. PBI membranes sandwiched between two PE layers were punched out manually to give a separator-membrane-separator stack with a diameter of 8 mm (**Figure 2b**). The membrane separator stack was then placed on a clean glass plate. The stack was then covered with electrolyte and covered with a top glass plate. In this configuration, the membrane was doped with electrolyte overnight (16 h) before the measurement (**Figure 2c**). To measure the membrane resistance, one PE-separator was carefully removed and the remaining PE-membrane bilayer was assembled into the measurement cell. Pressure was applied by tightening the PFA fittings of the cell. The cell resistance was determined by electrochemical impedance spectroscopy.

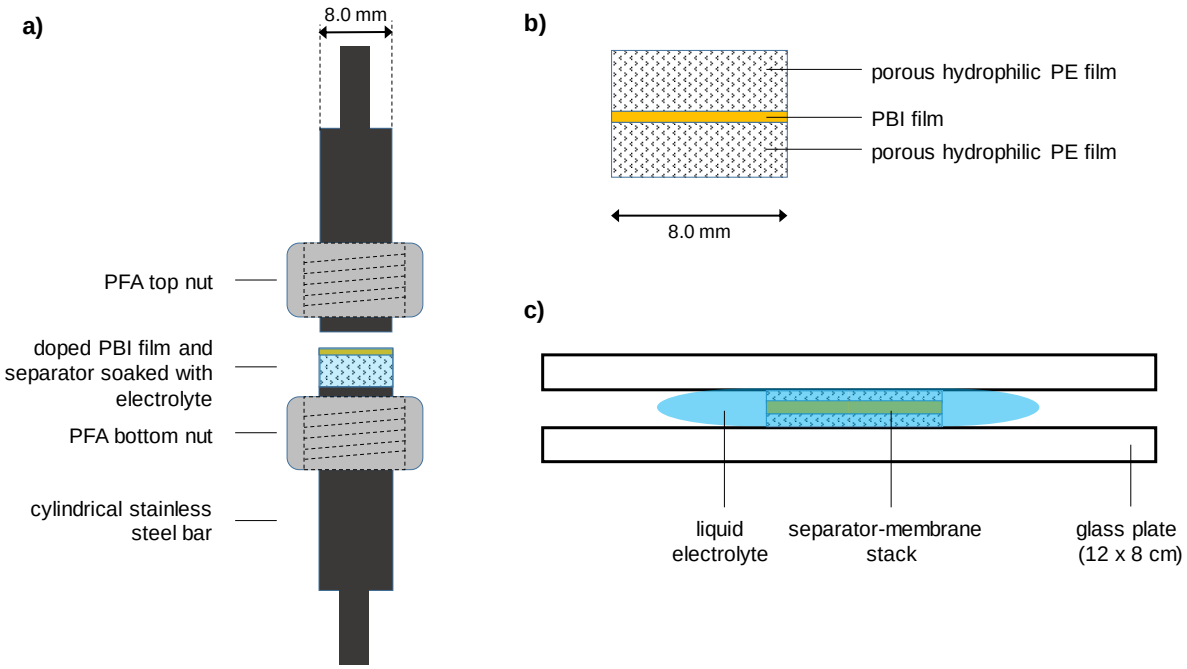


**Figure S2.** a) Samples of PBI with bottom and top layer of a hydrophilic microporous polyethylene (PE) film (Evopor™ 5E02A, Lydall Performance Materials, The Netherlands) were punched out to obtain sample discs with 8 mm diameter. b) Acid doping of the tri-layer overnight (16 h) using $V^{+3.5}$ electrolyte between two glass plates. c) Removal of one layer of PE, then the sample is assembled into the Swagelok cell to measure the high frequency resistance by electrochemical impedance spectroscopy.

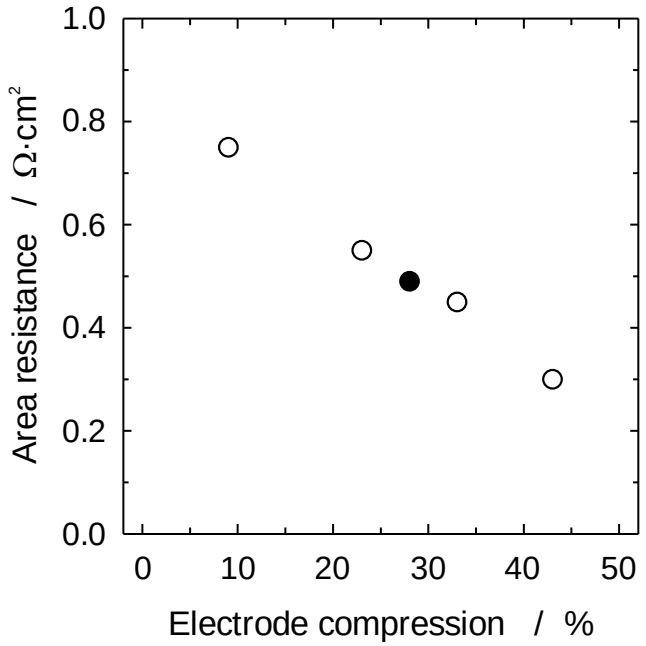


**Figure S3.** High frequency resistance measured with cell assembled with Toyobo carbon felt electrodes (type AAF304ZS, nominal thickness 4.3 mm) and a microporous polypropylene separator (TreoPore PDA-30). The compression was adjusted with cell frames of various thickness. $V^{+3.5}$ electrolyte was circulated through the cell compartments. The filled symbol indicates the compression used in cell tests (28 %).

**Table S2.** Thickness of free-standing dry PBI films. The uncertainty corresponds to 1 standard deviation. Numbers in brackets indicate the relative uncertainty.

| Sample | Thickness (□m) | |
|---|---|---|
| 1 | 0.22 ± 0.01 | (4.5 %) |
| 2 | 0.98 ± 0.02 | (2.4 %) |
| 3 | 2.91 ± 0.03 | (1.1 %) |
| 4 | 10.00 ± 0.08 | (0.8 %) |

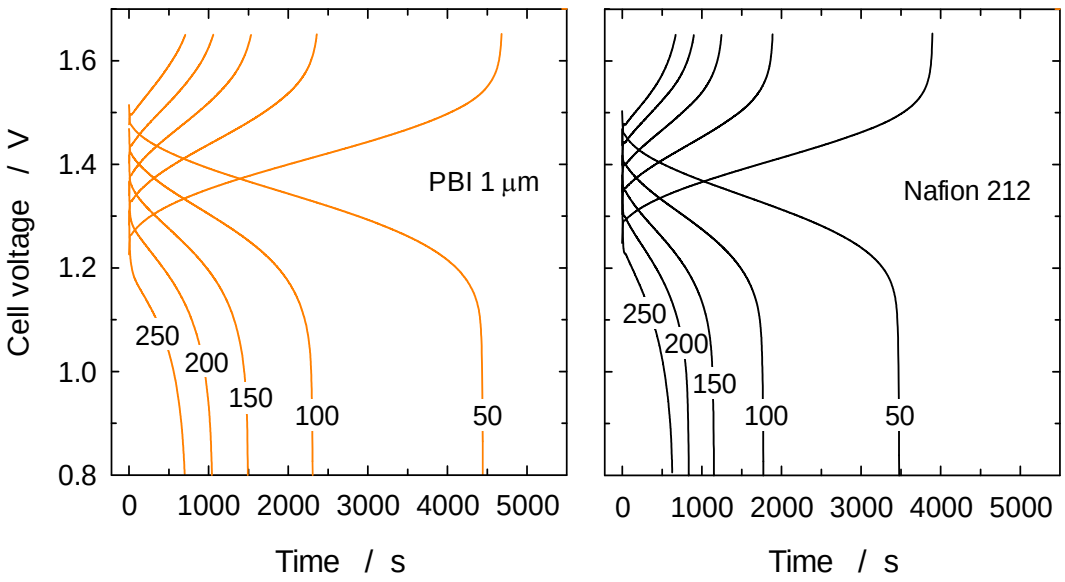


**Figure S4.** Charge/discharge curves recorded at room temperature. The numbers indicate the current density in mA□cm$^{-2}$. Electrodes: Toyobo AAF304ZS (compression: 28 %). 40 mL of vanadium electrolyte on each side (nominal capacity: 1.72 Ah), flow rate: 50 ml□min$^{-1}$.

**S5. Fitting of Efficiency Curves**

The parameters of a phenomenological model have been fitted to the data showing charge-discharge efficiencies as a function of current density in **Figure 4** of the main text. The model is based on the simplified description of coulombic and voltaic efficiencies by Xie et al.[1] The coulombic efficiency is approximated as:

$$\varepsilon_C \approx 1-(1+\tau)\frac{i_x}{i} \approx 1-2\frac{i_x}{i} \quad \text{(S1)}$$

where $i$ is the current density, $i_x$ the effective vanadium crossover current density, and $\tau$ the ratio of charge time $t_c$ to discharge time $t_d$, which can be approximated as 1 at coulombic efficiencies close to 100 %. With the resulting expression (Equation S1) the value of $\varepsilon_C$ approaches 100 % at high current densities. However, the data, as shown in **Figure S5**, typically approaches a maximum coulombic efficiency $\varepsilon_C^0$, which may be a result of asymmetric vanadium crossover during charge and discharge reactions or of hydrogen evolution taking place as a side reaction on the negative electrode during charging. Therefore, the fitting equation of the coulombic efficiency was modified as follows:

$$\varepsilon_C = \varepsilon_C^0 - 2\frac{i_x}{i} \quad \text{(S2)}$$

The expression is a hyperbolic function of the current density $i$. An analogous expression can be derived for the voltaic efficiency $\varepsilon_V$, which is a linear function of the current density $i$:

$$\varepsilon_V \approx 1-(1+\tau^{-1})\frac{R_\Omega}{U_0} i \approx 1-2\frac{R_\Omega}{U_0} i \quad \text{(S3)}$$

where $R_\Omega$ is the ohmic resistance and $U_0$ the open circuit voltage of the cell.[1] Here we also introduce a phenomenological parameter $\varepsilon_V^0$, which corresponds to the limit of the voltaic efficiency at zero current. Hence we obtain:

$$\varepsilon_V = \varepsilon_V^0 - 2\frac{R_\Omega}{U_0} i \quad \text{(S4)}$$

Obtained fitting parameters are given in **Table S3**.

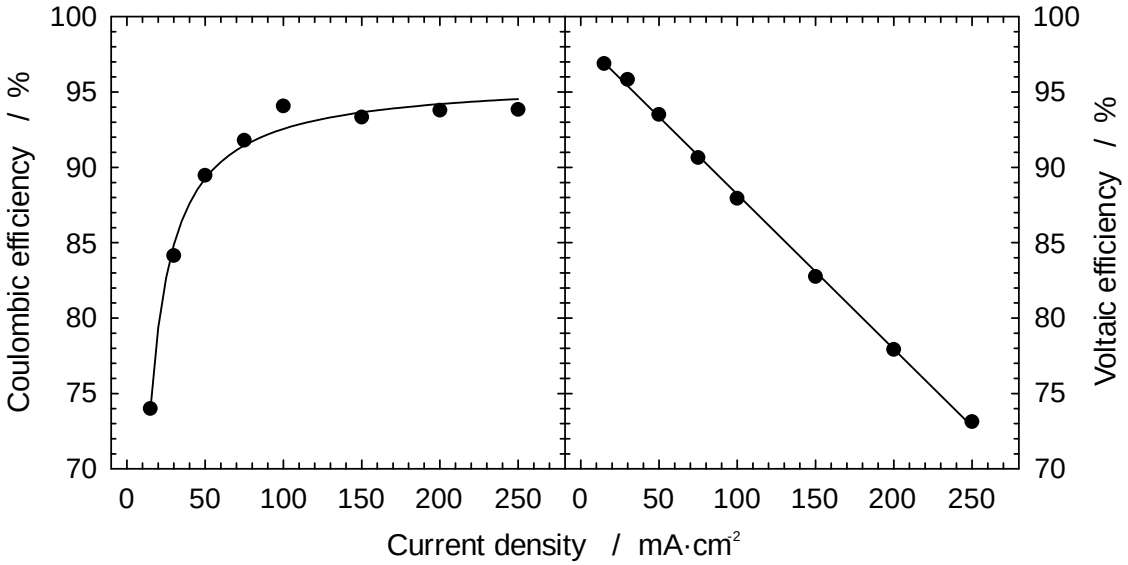


**Figure S5.** Efficiency data of the cell containing Nafion® 212 (main text, **Figure 4**) and fitted curves using **Equations S2** and **S4**, respectively.

**Table S3**. Results of curve fittings (**Equations S2** and **S4**) to efficiency data for cells with different membranes (data of **Figure 4** and Nafion® 115). The value of $U_0$ in **Equation S4** is arbitrarily set to 1.4 V.

| **Sample** | $i_x$ **(mA·cm$^{-2}$)** | $\varepsilon_C^0$ **(%)** | $R_{\square}$ **(□□cm$^2$)** | $\varepsilon_V^0$ **(%)** |
|---|---|---|---|---|
| PP-PBI(0.22 □m) | 1.1 | 98.6 | 0.71 | 99.2 |
| PP-PBI(0.98 □m) | 0.52 | 99.5 | 0.85 | 99.7 |
| PP-PBI(2.9 □m) | 0.28 | 100[b] | 1.2 | 99.6 |
| PP-PBI(10 □m) | $(2.7\cdot10^{-6})$[a] | 100[b] | 1.6 | 99.9 |
| Nafion® 212 | 1.6 | 95.7 | 0.70 | 98.3 |
| Nafion® 115 | 0.43 | 97.2 | 1.7 | 97.9 |

[a] high uncertainty
[b] value constrained to max. 100 %

## Reference

1. W. Xie, R. M. Darling and M. L. Perry, *J. Electrochem. Soc.*, **163**(1) A5084 (2016).